Journal of Applied Pharmaceutical Science Vol. 13(08), pp 140-150, August, 2023
Available online at http://www.japsonline.com
DOI: 10.7324/JAPS.2023.24237
ISSN 2231-3354

Development, characterization and optimization of solid lipid nanoparticles of alpha-mangostin by central composite design approach

Vutti Nagendra Babu[1], Gudhanti S. N. Koteswara Rao[2*], Roja Rani Budha[2,3], Rajasekhar Reddy Alavala[2], Prasanna Kumar Desu[1], Govada Kishore Babu[4], Arja Durga Prasad[4]

[1]Department of Pharmacy, Koneru Lakshmaiah Education Foundation, Vaddeswaram, India.
[2]Shobhaben Pratapbhai Patel School of Pharmacy & Technology Management, SVKM's NMIMS, Mumbai, India.
[3]Department of Pharmacology, Institute of Pharmaceutical Technology, Sri Padmavathi Mahila Visvavidyalayam, Tirupati, India.
[4]Formulation R&D, Laila Nutraceuticals, Vijayawada, India.

ARTICLE INFO

Received on: 22/03/2023
Accepted on: 17/07/2023
Available Online: 04/08/2023

Key words:
Central composite design, solid lipid nanoparticles, α-mangostin, hot melt homogenization, ultrasonication.

ABSTRACT

The study aims to formulate solid lipid nanoparticles (SLNPs) of the poorly bioavailable drug α-mangostin by central composite design and evaluate their *in-vitro* drug characteristics. The contribution of ingredients to the physicochemical characteristics of formulated SLNPs was investigated and further utilized to optimize the final formulation. For the formulation of SLNPs, hot melt homogenization method was used followed by a ultrasonication approach. The solid lipids used in the formulation include stearic acid and Precirol ATO5; the surfactant was Poloxamer 407, and the co-surfactant was sodium taurocholate to provide the negative charge. The optimized formulation's mean particle size, entrapment efficiency, zeta potential, and drug loading were 173.6 nm, 72.42%, −43.3 mV, and 20.46%, respectively. X-ray diffractometry confirms the amorphous nature of SLNPs. Scanning electron microscopy analysis showed spherical morphology and a particle size range between 145 and 218 nm. Differential scanning calorimetry and Fourier transform infrared studies confirmed the absence of drug-excipient interactions. According to the findings, the optimum surfactant and lipid combination produced high-quality SLNPs with stable release properties for at least 6 months at room and refrigerator temperatures. The obtained results encourage that SLNPs can be used as oral drug delivery carriers for α-Mangostin, because of their exceptional properties.

INTRODUCTION

The drug's therapeutic efficacy relies mostly on four fundamental mechanisms: absorption, distribution, metabolism, and excretion. Low therapeutic effectiveness is caused by limited solubility and permeability, low blood distribution volume, first pass and pre-systemic metabolism, faster elimination, and poor bioavailability. However, designing colloidal delivery systems does not boost therapeutic efficacy due to their instability and non-biodegradable delivery methods. With better stability, reduced toxicity, and biodegradability, developing a solid lipid nanoparticles (SLNPs) dosage form removes the drawbacks of traditional colloidal drug delivery methods (Delie and Blanco-Prieto, 2005). Lipophilic SLNPs entrap medicines with various physicochemical and pharmacological features in their lipid core (Anthony *et al*., 2012; Asif *et al*., 2022). Finally, the energy-independent transcellular transport mechanism delivers the entrapped drug to the active site.

"Autonomous fruit," *Garcinia mangosteena* originates in South Asia and is the best edible, tasty fruit (Zhao *et al*., 2016). α-mangostin is the major xanthone derivative, which is 75% of the total 200 xanthones isolated by a series of researchers from the

**Corresponding Author*
Gudhanti S. N. Koteswara Rao, Shobhaben Pratapbhai Patel School of Pharmacy & Technology Management, SVKM's NMIMS, Mumbai, India.
E-mail: drgsnkrao @ gmail.com

pericarp of the fruit. In traditional medicines, this α-mangostin is used as anti-tumor, anti-inflammatory, anti-allergic, anti-microbial, anti-bacterial, anti-fungal, anti-oxidant, analgesic, cardioprotective, and immunomodulator for many reasons (Kurose *et al*., 2012). α-mangostin is partly converted to phase-2 metabolites when it passed through the apical membrane of Caco-2 cells' enterocytes (Bumrungpert *et al*., 2009). In the cell lines HepG2, HT-29, Caco-2, and THP-1, mangostin conjugates underwent cellular transit and metabolism (Gutierrez-Orozco *et al*., 2013). When rats were given α-mangostin (20 mg/kg dosage) dissolved in an aqueous solution with 2% each of alcohol and Tween-80, bioavailability was found to be 0.4% following oral administration (Li *et al*., 2011). After 63 minutes of treatment of 40 mg/kg of α-mangostin in rats, the C_{max} (maximum plasma concentration) is reached (Syamsudin *et al*., 2010). α-mangostin acts as an anti-inflammatory agent for mediators like tumor necrotic factor and interleukin-6 (in human U937 macrophage-like cells) stimulated by lipo-polysaccharides (Gutierrez-Orozco *et al*., 2013).

Various formulations have been examined in the past as techniques to boost the solubility and bioavailability of the poorly soluble drugs, including lipid-based nanoparticles (Hassan *et al*., 2020), polymeric nanoparticulate systems (Basit *et al*., 2020), mixed micelles, and niosomal carriers (Akbarzadeh and Iman, 2020; Ghafelehbashi *et al*., 2019). To improve α-mangostin bioavailability (Ghosh *et al*., 2008), several attempts have been made to integrate it into other types of delivery systems, such as microemulsion (Pizzol *et al*., 2014), liposome (Chetoni *et al*., 2004), and nanoemulsion (Schwarz *et al*., 2012; Wathoni *et al*., 2020). The emulsion formulation, however, was not exceptionally stable during storage due to nanoparticle coalescence, with encapsulated material leakage and increased particle size (Ghosh *et al*., 2006). In the last decade, SLNP has been projected as a carrier for drug delivery with substantial advantages over typical colloidal drug carriers (Mehnert and Mader, 2001). However, because of its biocompatibility, biodegradability, and stability, this system is considered as an alternate delivery strategy that can overcome the pharmacokinetic restrictions of freshly manufactured and commercially available pharmaceuticals.

In addition, the ability of the SLNP to permeate epithelial cells offers protection of the apical surface against degradation of the entrapped drug and increased absorption of the active ingredients during oral drug delivery (Muchow *et al*., 2008; Muller and Keck, 2004). These findings show that SLNP has a more significant potential for delivery of drug over other carriers.

One of the most critical aspects of developing a successful nanocarrier system is its design and optimization. A nanoparticle formulation can be designed using a variety of techniques and procedures. The most common technique for studying the impact of composition and process parameters on quality features is to alter a particular variable while keeping the other variables constant. However, this method necessitates many experiments, and studying the interplay of components is challenging. Such experiments will be potentially misconceived (Hao *et al*., 2011).

To overcome this challenge, central composite design (CCD) of response surface methodologies (RSM) can be utilized throughout the design and development of a formulation to find the interaction impact of various aspects that influence product results or quality (responses). Furthermore, various studies have effectively employed CCD to create and optimize formulations, with CCD data demonstrating strong and trustworthy predictions (Gajic *et al*., 2021; Savic Gajic *et al*., 2019).

The effects of three independent variables, the concentration of stearic acid, Precirol ATO5 (solid lipid), Poloxamer-407, and sodium taurocholate (STC; surfactant), on four dependent variables (responses), mean particle size, entrapment efficiency (EE), drug loading, and zeta potential, were investigated using CCD in this study to optimize the SLNP formulation for encapsulation of α-mangostin.

MATERIALS AND METHODS

Materials

The drug α-mangostin was received from Laila Nutraceutical (Andhra Pradesh, India). Solid lipids, stearic acid was obtained from Finar chemicals (Gujarat, India), and Precirol ATO5 was obtained from Gattefose India Pvt. Ltd. (Mumbai, India). The surfactant poloxamer 407 was gifted by Muby Chemicals (Gujarat, India). All other ingredients used were of analytical grade.

Methodology

Central composite design

Design Expert® 13.0.9.0 version was used to create the CCD experiments, and a total of 20 statistical estimation trials were performed. The effect of variables and their respective responses were evaluated using the analysis of variance (ANOVA) with Fisher's test. The $p < 0.05$ level was deemed statistically significant. 3D surface plots were used to show the relationship between the factors and their respective responses. The high and low levels of the variables are shown in Table 1.

Statistical analysis

The ideal concentration of the independent variables (lipids and surfactant) for SLNP formulation was found to depend on the state of the responses in obtaining the smallest particle size, maximum encapsulation efficiency, maximum drug loading, and maximum zeta potential. The generalized response surface model and polynomial Equation (1) were used to explore the response behavior of the *Y*-response function.

$$Y = \beta_0 + \beta_1 x_1 + \beta_2 x_2 + \beta_3 x_3 + \beta_{11} x_1^2 + \beta_{22} x_2^2 + \beta_{33} x_2^2 + \beta_{12} x_1 x_2 + \beta_{23} x_2 x_3 + \beta_{13} x_1 x_3 \quad (1)$$

ANOVA examines the differences in factors. All insignificant variable effects ($p > 0.05$) were found in the simplified model. The interaction effects of the factors on their respective responses were depicted using 3D response plots.

Models are checked for accuracy

To validate and confirm the models, a quantitative comparison of the prediction and the experimental data was performed using the *t*-test. A *p*-value of less than 0.05 was considered significant.

Table 1. Factors for experiment design.

Three factors under investigation	Levels	
	Low	High
Concentration of lipid-1 (Stearic acid)(%w/w)	0.5	1.5
Concentration of lipid-2 (Precirol ATO5)(%w/w)	0.75	2.25
Similar ratio of poloxamer 407 and STC (%w/w)	1	2

SLNP formulation

Hot melt homogenization and ultrasonication were used to synthesize α-mangostin-SLNPs (Silva *et al*., 2011). Briefly, SLNPs were prepared by heating solid lipid to a melting temperature of 60°C–65°C (about 5°C above the solid lipid melting point). A high-speed stirrer was used to mix the liquefied lipid for 5 minutes at high rpm (15,000 rpm). Required quantity of α-mangostin was added to the molten liquid while stirring continuously at the same temperature and mixed well for another 5–10 minutes. To get a coarse emulsion, surfactant was mixed in distilled water and heated to a temperature of the lipid phase before being added to the molten lipid and homogenized at 15,000 rpm for 30 minutes. Finally, the pre-emulsion collected was sonicated at 50% amplitude for 3 minutes, with six 30-second intervals and a 1-minute time gap between intervals. After that, the emulsion was lyophilized in a freeze dryer for 24 hours using mannitol as a cryoprotectant. Before further evaluation, the formulations were cooled down and held in a 25°C chamber. The RSM regression process and statistical analysis provided by the Design Expert software were used to establish the perfect composition of the SLNP formulations.

Particle size, zeta potential and polydispersity index analysis

The formulation's particle size and zeta potential were determined using the dynamic light scattering (DLS) technique of a Malvern particle size analyzer (Malvern Nano ZS90, Worcs, UK) (Manjunath and Venkateswarlu, 2005). Before analysis, all samples were diluted in deionized water. The diluted samples were placed in cuvettes for particle size evaluation and injected for zeta potential evaluation by electrophoresis (capillary cells). At a temperature of 25°C ± 0.5°C and an incident angle of 90°, DLS data were recorded.

Drug EE and drug loading

Separating the free drug from SLNPs by ultrafiltration or centrifugation yielded high drug EE (Jawahar *et al*., 2009). The samples were diluted in water and centrifuged to remove impurities. The samples were centrifuged for 10 minutes at 4,000 rpm in a multifunction centrifuge. The quantity of untrapped α-mangostin in the supernatant collected after the centrifuge was measured using high performance liquid chromatography (HPLC) analysis set at 317 nm. The drug EE and drug loading were calculated using Equations (2) and (3):

$$\text{EE (\%)} = \frac{\text{(Total drug content in SLNP-Total free (untrapped)drug in SLNP) *100}}{\text{(Total drug content in SLNP)}} \quad (2)$$

$$\text{Drug loading (\%)} = \frac{\text{Drug weight in SLNP *100}}{\text{Total weight of SLNP}} \quad (3)$$

Fourier transform infrared (FT-IR) spectrophotometer analysis

The FT-IR spectrophotometer analysis was performed to determine any physical or chemical interactions between the formulation's components (Mills and Roberson, 1993). FT-IR analysis of potassium bromide pellets with α-mangostin was carried out in a Brucker FT-IR spectrometer at a 4,000–400 cm^{-1} range of spectra. Pellets containing 200 mg of potassium bromide and 2 mg of the sample were triturated homogeneously before being tested for analysis. The reference, pure α-mangostin, and α-mangostin SLNP were compared to see whether there was any incompatibility between the formulation components.

X-ray diffractometry (XRD)

The drug crystal lattice and its degree of crystallinity in the formulation are revealed by XRD analysis. It was used to examine the physical structure of the drug moiety in a formulation (crystalline or amorphous) on comparison with pure components (Agarwal *et al*., 2020; Chen *et al*., 2017). Using a Bruker D8 focus XRD with Nickle-filtered Copper-potassium radiation at a voltage of 40 kV and a current of 30 mA, the XRD spectra of pure and α-mangostin loaded SLNPs were obtained in the polymethyl methacrylate sample holder.

Differential scanning calorimetry (DSC)

Using a Mettler Toledo DSC 821E (Germany), a DSC analysis was done. Indium was used to calibrate the device's melting point and fusion heat (calibration reference: 99.9% pure). A 10°C/minute heating rate was utilized in the range of 30°C–300°C. A nitrogen purge (40 ml/minute) was used in the experiment. Weighed the required sample quantity and placed it in a standard aluminum pan, with a control pan being empty (Pani *et al*., 2011). DSC thermograms were used to investigate pure drug medicament and α-mangostin-loaded SLNPs.

Scanning electron microscopy (SEM)

A Hitachi S-3700N SEM was used to examine the appearance of the SLNPs. A light sprinkling of SLNPs on a double adhesive carbon tape attached to an Al stub was used to prepare samples for SEM analysis. In an argon environment, the stub was then covered with gold to a thickness of 500 μ using a gold sputtering module in a high vacuum evaporator. After that, the samples were scanned, and photo-micrographs were obtained at magnifications of 11,000×.

Reverse phase (RP)-HPLC method

A RP-HPLC method was developed and validated for quantitative estimation of α-mangostin extracted from SLNPs of α-mangostin. Alliance e2695 instruments with Empower-3 analysis software with Quaternary gradient pump, autosampler with X-Bridge C18 Colum packed with octadecyl silane with porous 3.5 μm particles, 100 × 4.6 mm dimensions stationary column used for separation of eluents. Acetonitrile and 0.1% v/v orthophosphoric acid in 65:35 volumes was used as mobile phase at a flow rate of 1 ml/minute at a wavelength of 317 nm by a photodiode array detector.

In-vitro release study

In-vitro drug release studies of α-mangostin-loaded SLNPs were carried out without enzyme in simulated gastrointestinal fluid (SGF pH-1.2) and intestinal fluid (SIF pH-6.8) buffers. The optimized α-mangostin-loaded SLNPs were put into a dialysis bag (cellulose membrane, 12,000 da), immersed

in 50 ml of release media at 100 rpm, and kept at 37°C ± 0.5°C throughout the study. 2 ml aliquots of release medium were taken from the beaker at various time intervals (30, 60 minutes, 2, 4, 6, 8, 12, 18 and 24 hours). In addition, collected samples were replaced with fresh buffers for maintaining sink conditions. The amount of α-mangostin released from the dialysis bag was determined by HPLC analysis at 317 nm wavelength (Alliance e2695 instruments with Empower-3 analysis software).

Short-term stability studies

All SLNP samples were maintained for 6 months in an amber-colored container at three different temperature and humidity conditions: 4°C ± 1°C (60% RH), 25°C ± 1°C (60% RH), and 40°C ± 2°C (75% RH) in a stability chamber, as defined in earlier research with minor modifications. The zeta potential, mean particle size, EE, and drug loading were all measured on a monthly basis.

RESULTS AND DISCUSSION

Results

Response surface model fitting

The RSM was used to estimate the zeta potential, mean particle size, EE, and drug loading of SLNP, which all depend on the ingredients used in the preparation of SLNPs. Data were statistically analyzed and used to build the best response model for the factors of the SLNP. Table 2 displays the *p*-values, *F*-values, and regression coefficients (R^2), with adequate precision, and derived equations.

ANOVA was used to evaluate the significance of the developed polynomial models (quadratic) (Table 3). All factors in the design had a big *F*-value and a modest *p*-value ($p < 0.05$), indicating that they had a substantial impact on the variables or factors. For example, stearic acid (solid lipid) strongly influenced the mean particle size, drug loading, and zeta potential compared with other solid lipids and surfactants. The surfactant concentration, on the other hand, had a significant impact on the EE of SLNP when compared to solid lipids, according to the data. The interaction between surfactant (including co-surfactant) and the solid lipid had a substantial impact on mean particle size, EE, drug loading, and the zeta potential index of SLNP. The 3D-response plots of the combination of surfactant (including co-surfactant) and the solid lipid revealed more about the interplay amongst the ingredients (Fig. 1).

The mean particle size, zeta potential, and poly dispersibility index (PDI) were improved when the concentration of surfactant (including co-surfactant) and the solid lipid was increased. Low surfactant concentrations can lead to smaller particle sizes, a lower PDI, and lower zeta potential in formulations. Mean particle size, EE, and drug loading, increased as the concentration of solid lipid increases. Increased surfactant concentration reduced particle size, drug loading, and EE.EE, drug loading, and zeta potential, all are improved when lipids and surfactants are present in large concentrations. As a result, there is a decrease in particle size.

Response surface model verification

Between predicted and observed values no significant ($p < 0.05$) difference is observed in the response models for the final formulation containing surfactant (including co-surfactant) and solid lipid (Tables 4–6).

Physical characteristics and EE

α-mangostin-loaded SLNP had a high percentage of drug entrapment, at 72.42%. Using a DLS approach, the mean particle size, drug loading, and zeta potential of α-mangostin-loaded SLNP were found to be 173.6 nm, 20.46%, and −42.3 mV, respectively. According to the data, the physical features of the SLNP system were not considerably affected by the addition of α-mangostin.

Scanning electron microscopy

The mean particle size of the SLNP loaded α-mangostin under a SEM was less than 225 nm (average-173.72 nm), which was consistent with the design 95% confidence interval range of 148.53–186.38 nm and close to the particle size data (173.6 nm). The particle size distribution in all samples was well-dispersed and uniform, with the usual spherical shape of SLNP. Figure 2 shows the SEM α-mangostin-SLNP at 11,000× magnification.

FT-IR spectrophotometry analysis

The FT-IR spectra of the reference, α-mangostin, and αM-SLNP are almost identical with minor differences, indicating no physicochemical interactions between the formulation components. Table 7 and Figure 3 summarize the findings.

DSC analysis

α-mangostin has a melting temperature of 181°C–182°C. A confirmatory test was done before SLNP creation and optimization, and the pure α-mangostin compound displayed a peak at 195.98°C, which is close to the reported values. The SLNP

Table 2. Regression coefficient and equation for the response surface model.

Response	*p*-value	*F*-value	R^2-value	Adequate precision	Regression coefficient equation
Particle size	0.0008	9.51	0.895	10.788	243.055 + 11.5587 * A + 62.5503 * B − 118.456 * C + 2.7 * AB − 52.55 * AC − 115.9 * BC + 69.2094 * A^2 + 29.4712 * B^2 + 103.363 * C^2
Zeta potential	0.017	4.28	0.794	6.429	39.679 + 4.59131 * A − 6.99609 * B + 4.72149 * C + 0.866667 * AB + 2.9 * AC + 9.6 * BC − 6.51056 * A^2 − 2.10791 * B^2 − 6.43985 * C^2
EE	0.009	5.14	0.822	8.728	57.4366 + 15.9366 * A + 7.24006 * B − 6.16707 * C + 0.09 * AB − 0.215 * AC + 1.13 * BC − 4.68055 * A^2 − 2.18395 * B^2 + 4.13707 * C^2
%Drug loading	<0.00001	16.35	0.936	13.819	24.7023 − 1.54466 * A − 2.83341 * B − 0.545214 * C − 0.133333 * AB − 0.4 * AC + 0.0666 * BC − 0.408282 * A^2 + 0.415654 * B^2 + 0.298825 * C^2

Table 3. ANOVA regression coefficient terms for fitted model.

Variable effect	Source	Mean Particle size		Zeta potential		EE%		Drug loading %	
		F-value	*p*-value	*F*-value	*p*-value	*F*-value	*p*-value	*F*-value	*p*-value
	Models	**9.51**	**0.0008**	**4.28**	**0.017**	**5.140**	**0.009**	**16.35**	**<0.0001**
Linear effect	A-Concentration of stearic acid	28.40	0.0003	3.77	0.081	14.26	0.004	90.52	<0.0001
	B-Concentration of Precirol ATO5	4.60	0.058	4.16	0.069	4.81	0.053	53.47	<0.0001
	C-Equal ratio of Poloxamer 407 : STC	6.07	0.034	3.56	0.089	20.84	0.001	0.024	0.881
Interaction effect	AB	0.012	0.915	0.1207	0.736	0.0009	0.976	0.053	0.823
	AC	2.03	0.185	0.6004	0.456	0.002	0.962	0.212	0.655
	BC	22.23	0.001	14.80	0.003	0.147	0.709	0.013	0.911
Quadratic effect	A^2	6.35	0.030	5.45	0.042	2.02	0.186	0.398	0.542
	B^2	5.82	0.037	2.89	0.119	2.23	0.167	2.090	0.179
	C^2	14.15	0.004	5.33	0.044	1.58	0.238	0.213	0.654

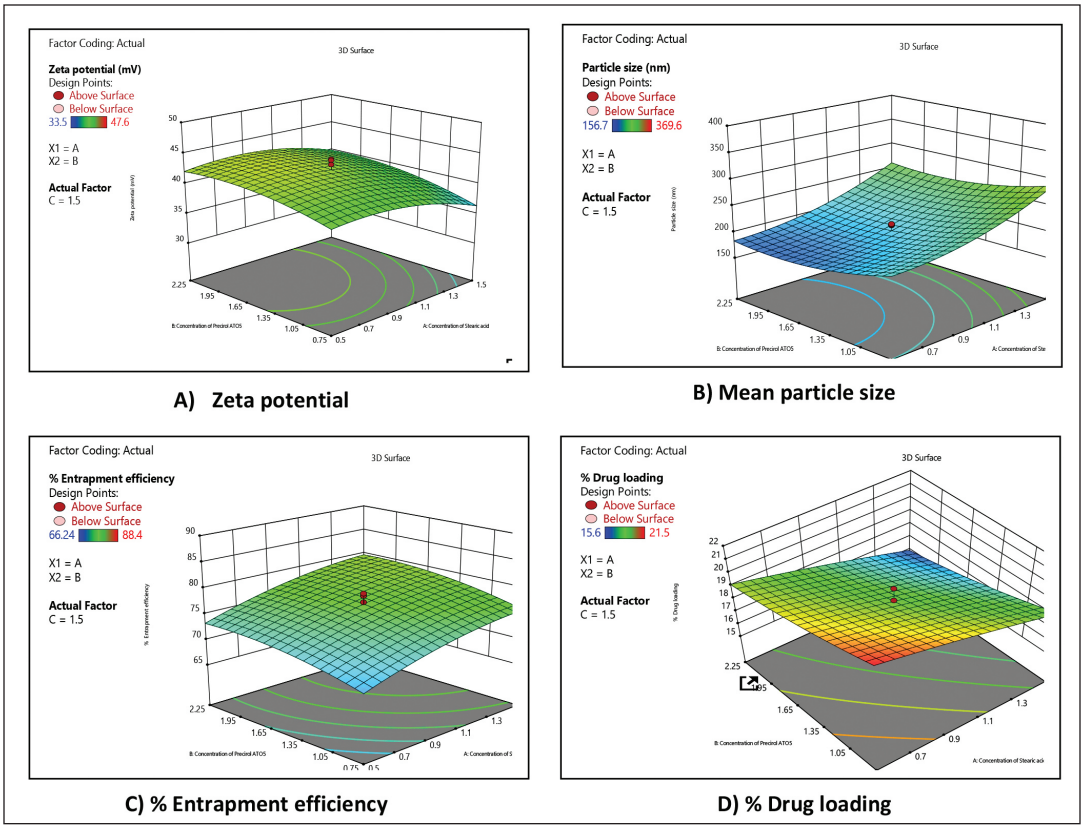

Figure 1. Response plots (3D) showing the effect of interaction between the lipids and surfactants on the (A) zeta potential, (B) particle size, (C) EE%, and (D) drug loading %.

prepared by hot melt homogenization followed by ultra-sonication technique showed an endothermic peak at 165.78°C, which is appropriate because α-mangostin changed its crystalline nature to an amorphous form during the preparation of nanoparticle. The pure α-mangostin and α-mangostin-loaded SLNP had a modest temperature decrease from 195.98°C to 165.78°C, respectively, on the thermogram (Fig. 4), showing an interaction between lipid and surfactant.

Table 4. Optimized formulation of SLNP.

Factor	Name	Level
A	Stearic acid	0.687
B	Precirol-ATO5	0.959
C	1:1ratio of Poloxamer-407: STC	1.178

Table 5. Optimized formulation response values.

Parameter	Predicted values	95% PI low	95% PI high	Observed values
Particle size (nm)	202.956	174.799	231.125	173.6 ± 11.02
Zeta potential (mV)	−41.501	38.643	44.359	−42.3 ± 1.77
% EE	70.748	67.372	74.125	72.42 ± 1.98
% Drug loading	20.55	19.887	21.213	20.46 ± 0.59

Table 6. Coefficient table for predicted and observed values of α-mangostin-Loaded SLNP.

Dependent variable	Stearic acid	Precirol ATO5	Poloxamer 407 : STC
Particle size	37.601	−15.140	−17.384
p-values	0.0003	0.058	0.034
Zeta potential	−1.389	1.460	1.351
p-values	0.081	0.069	0.089
% EE	3.194	1.855	3.862
p-values	0.004	0.053	0.001
% Drug loading	−1.581	−1.215	0.026
p-values	<0.0001	<0.0001	0.881

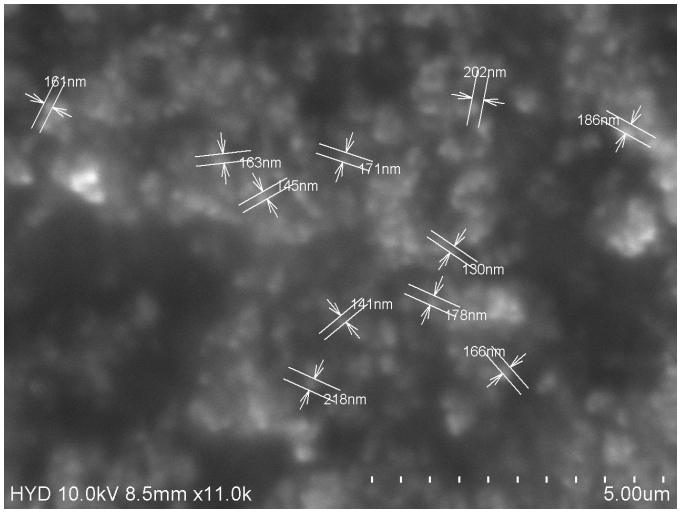

Figure 2. SEM analysis report of α-mangostin SLNPs.

X-ray diffractometry

The nature of α-mangsotin crystallinity was demonstrated by the distinctive peaks of pure extract and α-mangostin-SLNPs on the diffraction spectrum (Fig. 5). The α-mangostin loaded SLNPs formulation did not reveal the typical peaks of pure extract, showing that SLNPs are amorphous. The typical peaks of pure lipids were seen with lower intensity in α-mangostin-SLNPs formulation, confirming the reduced crystallinity of lipids in SLNPs. It reflects the amorphous form of the SLNPs that evolved. This will be owing to the SLNPs formulation's composition and the microemulsion technology utilized to manufacture it.

Short-term stability test

The results of stability studies were presented in Table 8. SLNPs were found to be stable at temperature of 4°C and 25°C because of steric hindrance and repulsive force provided by the surfactants over the apical surface of the SLNPs (Pizzol *et al*., 2014).

RP-HPLC method

Linearity was established within the concentration range of 17.38–260.90 µg/ml with R^2 value 0.999. Precision was attained with interday and intraday variations with a relative standard deviation of 0.048%–0.165% and 0.036%–0.182%, respectively.

In-vitro release study

When tested at a pH of 1.2-SGF and 6.8-SIF, the release profile of α-mangostin from SLNPs dispersion revealed a bi-phasic release pattern with an initial 20% release after the first 2 hours of the study, with the remainder released during the next 24 hours (Fig. 6). For pH 1.2 and 6.8, the two α-mangostin-loaded SLNPs graphs were practically overlaid. Results are given in Table 9.

DISCUSSION

CCD can be used to understand better how a single component's strength and its interactions affect the responses while designing SLNPs formulations. When the lipid concentration increased during the study, there is an increase in viscosity of the lipid phase apart from increased resistance to the flow of lipid, and the breakdown of lipid droplets at this viscosity is difficult, which led to an increase in particle size of the formulated SLNPs (Padhye and Nagarsenker, 2013; Zainol *et al*., 2012). Surfactant concentration is also critical to prevent particles of SLNPs from aggregating and to decrease the rate of collision of the particles; optimum surfactant concentration is required on the surface of the particles to prevent the collision and aggregation of the particles (Zirak and Pezeshki, 2015). Further, an increased concentration of surfactant results in increased PDI value due to non-uniformity of the micelles in the mixture, which is observed in this study (Mohtar *et al*., 2015). Aggregation and collision rate were also

Table 7. FT-IR spectral wave number data of reference, pure α-mangostin and α-mangostin-SLNP (in cm^{-1}).

Type of interaction	FT-IR data (Reference)	FT-IR data (Pure active)	FT-IR data (αM-SLNP)
(–CH_2 stretching vibration)	2,922 cm^{-1}	2,920	2,914.5
(C=C un-conjugated stretching vibration)	1,654 cm^{-1}	1,604	1,605.13
(CH_2 bending)	1,409 cm^{-1}	1,456	1,467.93
(CH_3 bending)	1,367 cm^{-1}	1,373	1,382.54
(C–O stretching vibration)	1,278 cm^{-1}	1,278	1,289.64
(C–OH stretching)	1,011 cm^{-1}	1,080	1,019.02
(–(CH_2)n)	772 cm^{-1}	774	759.60
(–HC=CH– bending)	677 cm^{-1}	612	688.35

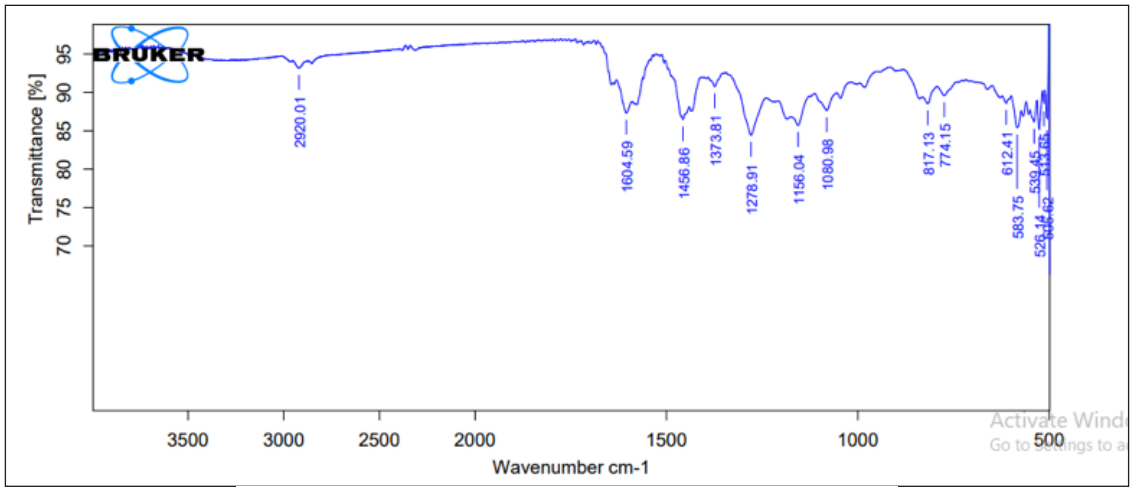

A) FT-IR Spectra of Pure α-Mangostin

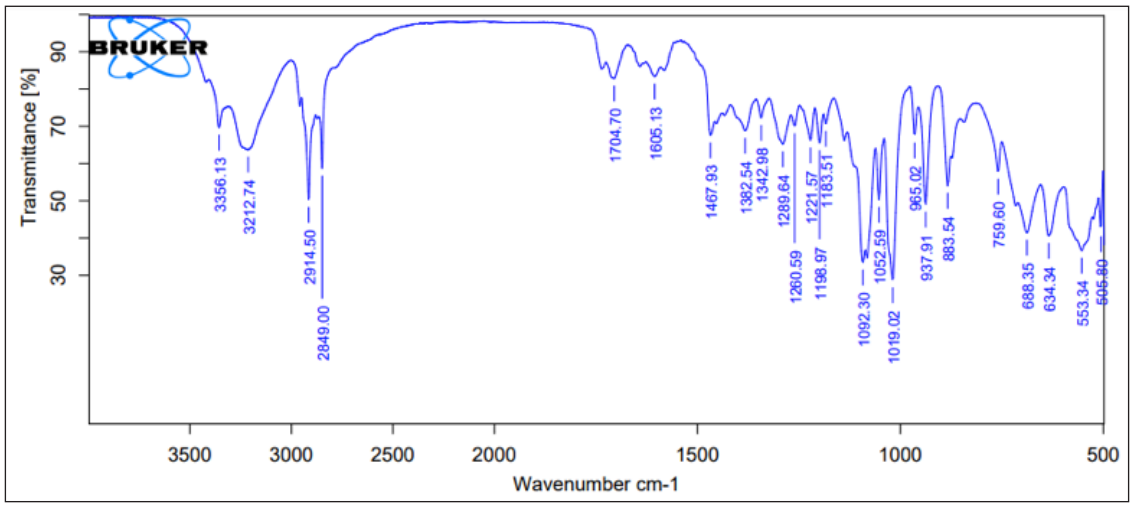

B) FT-IR Spectra of formulated α-Mangostin SLNP

Figure 3. FT-IR Spectra of α-mangostin and formulated α-mangostin SLNPs.

observed. There is variation in the emulsification efficiency of the surfactants at higher concentrations, which can lead to instability of the formulation. Hence, it is important to maintain the concentration of surfactant at an optimal level, which can prevent varying particle sizes of the particles by preventing aggregation. SLNPs smaller particle size and PDI concentration of lipid and the surfactant should be ideal for formulation stability. Zeta potential value alters at a high concentration of the surfactant due to the hiding of charge on the particle's surface (Asasutjari *et al*., 2013) and further reduction of the value of zeta potential (Asasutjarit *et al*., 2007). Factors that have quadratic model interactions will influence the responses. From SEM analysis, formulated SLNPs

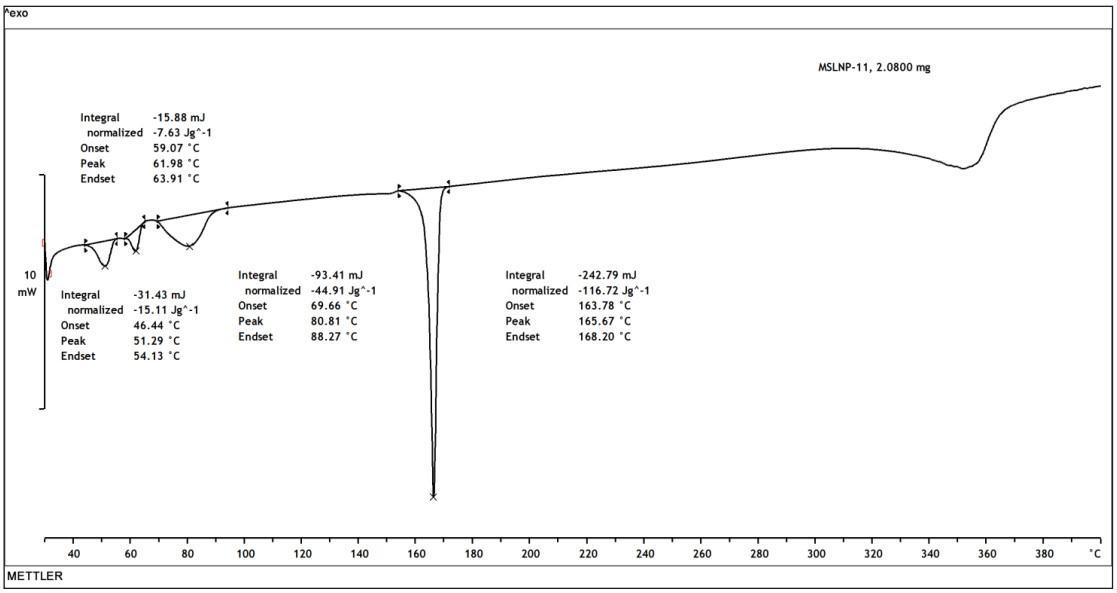

Figure 4. DSC thermogram of α-mangostin-SLNPs.

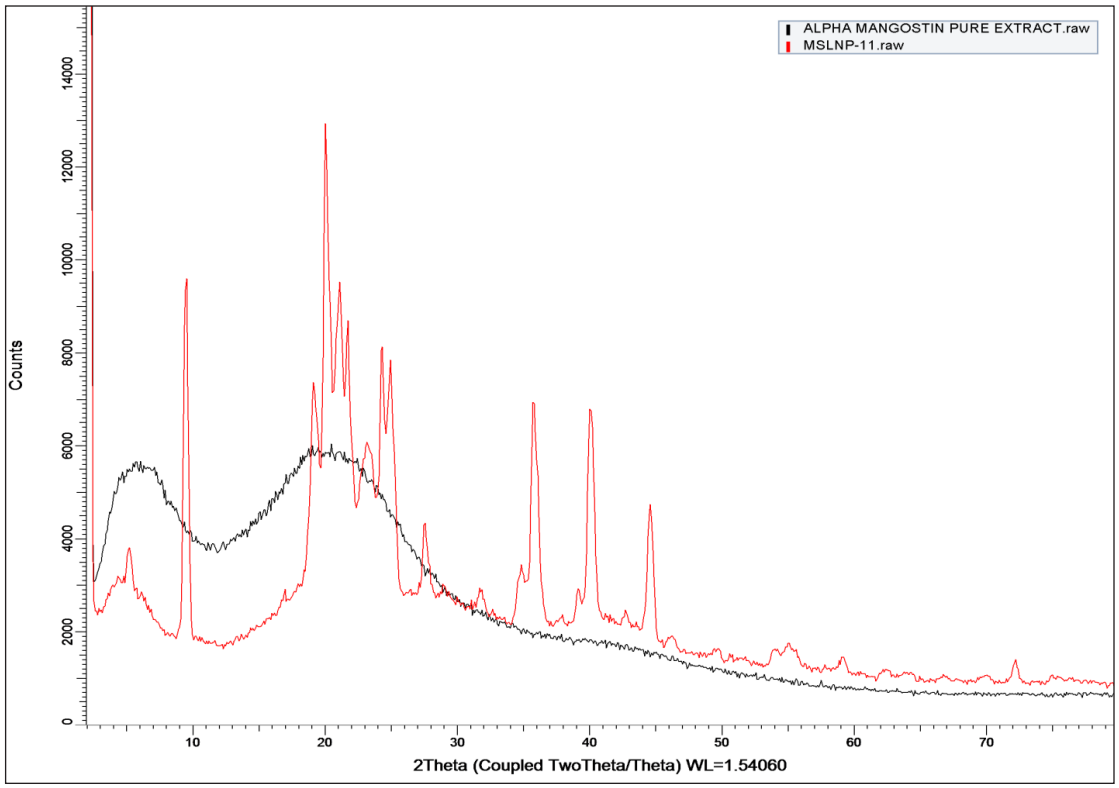

Figure 5. XRD of Pure α-mangostin and α-mangostin-SLNPs.

of α-mangostin showed particles of uniform shape (spherical) with smooth particle surface. α-mangostin was entrapped at higher level during the formulation of SLNPs in the lipid matrix, which is confirmed by the results of high EE of a drug (Seyfoddin and Al-Kassas, 2012). The generous space available for a drug molecule in a lipid matrix was low even after the small addition of the drug to the lipid (Mohtar *et al*., 2015). The high α-mangostin encapsulation efficiency obtained in this design was observed with by the right combination of Precirol ATO5 and stearic acid. The thermogram of the lipid in α-mangostin-loaded SLNPs revealed a lower melting temperature than their bulk lipid equivalent, indicating a surfactant-solid lipid interaction (Bunjes and Unruh, 2007). The energy required to break the crystal with a structured lattice is high compared to crystals with irregular and damaged

Table 8. Mean particle size, EE, zeta potential and drug loading measurements of SLNP formulations stored at 4°C, 25°C and 40°C.

Evaluation parameter	Storage conditions	Time intervals in months			
		First month	Second month	Third month	Sixth month
Mean particle size (nm)	4°C ± 1°C	190.40	218.20	226.60	231.70
	25°C/60%RH	221.60	239.80	247.10	265.30
	40°C/75%RH	240.30	295.30	389.20	511.20
EE%	4°C ± 1°C	70.69	76.90	75.54	73.82
	25°C/60%RH	71.64	73.27	72.14	67.73
	40°C/75%RH	69.22	62.03	57.77	45.08
Zeta potential (mV)	4°C ± 1°C	42.16	−39.29	−37.84	−34.83
	25°C/60%RH	−40.31	−37.18	−34.73	−32.72
	40°C/75%RH	−40.69	−34.07	−32.62	−27.61
Drug loading%	4°C ± 1°C	20.16	19.46	18.91	18.58
	25°C/60% RH	19.61	19.12	18.18	17.65
	40°C/75% RH	18.94	18.31	17.34	15.74

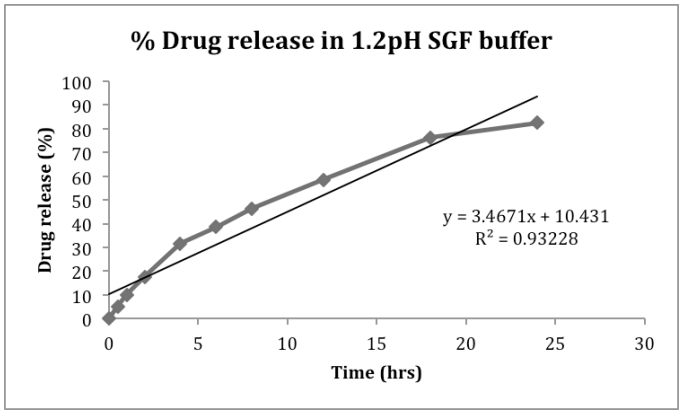

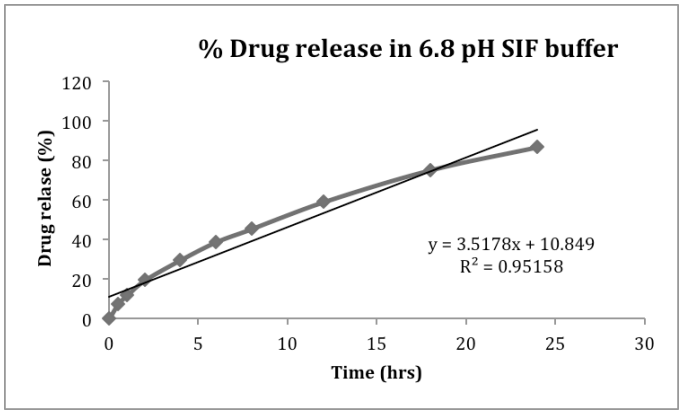

Figure 6. *In-vitro* α-Mangostin release profiles from α-mangostin -loaded SLNPs at (a) pH of 1.2 and (b) pH of 6.8.

lattices. Hence the lipid loses its crystallinity at this operational energy and becomes amorphous lipids that are less ordered in arrangement and have lower melting temperature than native crystals (Neves *et al*., 2013; Westesen *et al*., 1993). Information on the degree of crystallinity and arrangement order is critical as these parameters influence the EE of the formulation and drug release at a controlled rate. Less ordered crystalline nature favors good

Table 9. *In-vitro* α-mangostin release correlation coefficient data of α-mangostin SLNPs in different pH buffers.

Release model		1.2 pH SGF Buffer	6.8 pH SIF Buffer
Zero order	R^2	**0.932**	**0.951**
First order	R^2	0.571	0.558
Higuchi	R^2	**0.990**	**0.994**
Korsmeyer-peppas-plot	R^2	0.988	0.998
	n	**0.666**	**0.625**

The high R^2 and n-value indicates a zero order kinetics with non-fickian diffusion mechanism of drug release.

EE and controlled release (Souto *et al*., 2005; Vivek *et al*., 2007). The optimized formulation was evaluated for its *in-vitro* release in pH 1.2-SGF and 6.8-SIF buffer at the temperature of 37°C ± 0.5°C. No effective difference was observed in the release profile at both pH buffers from the findings. Around 20% of the drug is released in the first 2 hours of the study, suggesting the release of unentrapped drug (surface bound). This kind of surface-bound phenomenon is generally found in the hot melt homogenization technique, where a drug can partition into the aqueous phase of the emulsifier during high-temperature processing and further reduce the drug available in the lipid melt core. This process of partitioning into the aqueous phase will be reversed to the lipid phase, which will eventually increase drug availability in the lipid core (Mohtar *et al*., 2015; Muller *et al*., 2000). Further drug release from the lipid core is controlled over time, suggesting the partition process is reversed (Silva *et al*., 2012). To avoid photolytic degradation and interference of the light on the formulation stability the prepared SLNPs been stored in amber color bottles before performing stability studies. SLNPs were found to be stable at a temperature of 4°C and 25°C because of steric hindrance and repulsive force provided by the surfactants over the apical surface of the SLNPs (Pizzol *et al*., 2014). The low stability of the formulation at 40°C might be due to a decrease in viscosity of the emulsion as the micro-viscosity (film layer that prevents coalescence) ruptures and alters steric hindrance, and promote adhesion of the particles to one another. This could reduce the stability of the particles, which

was confirmed by the decrease in the value of zeta potential during the duration of the study. The stability of the formulation is greater only when the attractive forces (like Vander wals forces) are less than repulsive forces from the surface of the particle (Muller *et al*., 2000). The change in lipid crystalline nature at a high temperature was witnessed with the decrease in zeta potential value. Particle matrices that have been re-oriented influence particle surface charges, leading zeta potential values to fluctuate. An increased kinetic energy of the particles during stability studies at high temperature resulted in dominative repulsive forces which might have caused aggregation of particles by collision (Freitas and Muller, 1998; Shah *et al*., 2014).

CONCLUSION

Based on the current investigation and respective findings it was concluded that CCD was successfully applied to develop the SLNPs of α-mangostin. The interplay between surfactant (including co-surfactant) and solid lipid as the critical components of SLNPs formulation and their impact on mean particle size, zeta potential, EE, and drug loading were better understood using the response plots (3D) developed in this study. The optimized formulation of SLNPs were found to be stable for 6 months at both 4°C and 25°C. CCD has developed SLNPs of α-mangostin with high percentage of EE. Furthermore, the α-mangostin-loaded SLNPs were found to show controlled drug release of the drug.

ACKNOWLEDGMENT

Authors are thankful to Laila Nutraceuticals R&D, Vijayawada, India for providing necessary facilities to complete the current research work. Authors also thank Koneru Lakshmaiah Education Foundation, Vaddeswaram, India for providing guidance.

AUTHOR CONTRIBUTIONS

All authors made substantial contributions to conception and design, acquisition of data, or analysis and interpretation of data; participation in the writing of the article or critical revision of it for essential intellectual content; agreement to submit to the current journal; final approval of the version to be published; and agreement to be accountable for all parts of the work. According to the requirements/guidelines of the International Committee of Medical Journal Editors (ICMJE), all writers are entitled to be authors.

FINANCIAL SUPPORT

There is no funding to report.

CONFLICTS OF INTEREST

The authors report no financial or any other conflicts of interest in this work.

ETHICAL APPROVALS

This study does not involve experiments on animals or human subjects.

DATA AVAILABILITY

All data generated and analyzed are included in this research article.

PUBLISHER'S NOTE

This journal remains neutral with regard to jurisdictional claims in published institutional affiliation.

REFERNCES

Agarwal S, Murthy RSR, Harikumar SL, Garg R. Quality by design approach for development and characterisation of solid lipid nanoparticles of quetiapine fumarate. Curr Comput Aided Drug Des, 2020; 16(1):73–91.

Akbarzadeh I, Yaraki MT, Ahmadi S, Chiani M, Nourouzian D. Folic acid-functionalized niosomal nanoparticles for selective dual-drug delivery into breast cancer cells: an *in-vitro* investigation. Adv Powder Tech, 2020; 31(9):4064–71.

Asasutjari R, Sorrachaitawatwong C, Tipchuwong N, Pouthai S. Effect of formulation compositions on particle size and zeta potential of diclofenac sodium-loaded chitosan nanoparticles. Int J Pharmacol Pharm Sci, 2013; 7(9):568–70.

Asasutjarit R, Lorenzen S, Sirivichayakul S, Ruxrungtham K, Ruktanonchai U, Ritthidej GC. Effect of solid lipid nanoparticles formulation compositions on their size, zeta potential and potential for *in-vitro* pHIS-HIV-Hugag transfection. Pharm Res, 2007; 24(6):1098–107.

Asif AH, Desu PK, Alavala RR, Rao GSNK, Sreeharsha N, Meravanige G. Development, statistical optimization and characterization of fluvastatin loaded solid lipid nanoparticles: a 3^2 factorial design approach. Pharmaceutics, 2022; 14(3):584.

Anthony AA, Momoh MA, Builders PF. Lipid Nanoparticulate drug delivery systems: a revolution in dosage form design and development. Recent advances in novel drug carrier systems. IntechOpen, London, UK, 2012.

Bumrungpert A, Kalpravidh RW, Suksamrarn S, Chaivisuthangkura A, Chitchumroonchokchai C, Failla ML. Bioaccessibility, biotransformation, and transport of alpha-mangostin from Garcinia mangostana (Mangosteen) using simulated digestion and Caco-2 human intestinal cells. Mol Nutr Food Res, 2009; 53(1):S54–61.

Basit HM, Mohd Amin MCI, Ng SF, Katas H, Shah SU, Khan NR. Formulation and evaluation of microwave-modified chitosan-curcumin nanoparticles-a promising nanomaterials platform for skin tissue regeneration applications following burn wounds. Polymers (Basel), 2020; 12(11):2608.

Bunjes H, Unruh T. Characterization of lipid nanoparticles by differential scanning calorimetry, X-ray and neutron scattering. Adv Drug Deliv Rev, 2007; 59(6):379–402.

Chen Y, Zhang X, Wang B, Lv M, Zhu Y, Gao J. Fabrication and characterization of novel shape-stabilized stearic acid composite phase change materials with tannic-acid-templated mesoporous silica nanoparticles for thermal energy storage. RSC Adv, 2017; 7(26):15625–31.

Chetoni P, Rossi S, Burgalassi S, Monti D, Mariotti S, Saettone MF. Comparison of liposome-encapsulated alpha-mangostin with alpha-mangostin ointment: ocular pharmacokinetics in rabbits. J Ocul Pharmacol Ther, 2004; 20(2):169–77.

Delie F, Blanco-Prieto MJ. Polymeric particulates to improve the oral bioavailability of peptide drugs. Molecules, 2005; 10(1):65–80.

Freitas C, Muller RH. Effect of light and temperature on zeta potential and physical stability in solid lipid nanoparticle (SLN) dispersions. Int J Pharm, 1998; 168(2):221–9.

Gajic IS, Savic I, Gajic D, Dosic A. Ultrasound-assisted extraction of carotenoids from orange peel using olive oil and its encapsulation in ca-alginate beads. Biomolecules, 2021; 11(2):225.

Ghafelehbashi R, Akbarzadeh I, TavakkoliYaraki M, Lajevardi A, Fatemizadeh M, HeidarpoorSaremi L. Preparation, physicochemical properties, *in vitro* evaluation and release behavior of cephalexin-loaded niosomes. Int J Pharm, 2019; 569:118580.

Ghosh PK, Majithiya RJ, Umrethia ML, Murthy RS. Design and development of microemulsion drug delivery system of alpha-mangostin for improvement of oral bioavailability. AAPS Pharm Sci Tech, 2006; 7(3):77.

Ghosh S, Jhanji V, Lamoureux E, Taylor HR, Vajpayee RB. Acyclovir therapy in prevention of recurrent herpetic keratitis following penetrating keratoplasty. Am J Ophthalmol, 2008; 145(2):198–202.

Gutierrez-Orozco F, Chitchumroonchokchai C, Lesinski GB, Suksamrarn S, Failla ML. α-Mangostin: anti-inflammatory activity and metabolism by human cells. J Agric Food Chem, 2013; 61(16):3891–900.

Hao J, Fang X, Zhou Y, Wang J, Guo F, Li F, Peng X. Development and optimization of solid lipid nanoparticle formulation for ophthalmic delivery of chloramphenicol using a Box-Behnken design. Int J Nanomed, 2011; 6:683–92.

Hassan H, Bello RO, Adam SK, Alias E, Meor Mohd Affandi MMR, Shamsuddin AF, Basir R. Acyclovir-loaded solid lipid nanoparticles: optimization, characterization and evaluation of its pharmacokinetic profile. Nanomaterials, 2020; 10(9):1785.

Li L, Brunner I, Han AR, Hamburger M, Kinghorn AD, Frye R, Butterweck V. Pharmacokinetics of α-mangostin in rats after intravenous and oral application. Mol Nutr Food Res, 2011; 55(1):S67–74.

Jawahar N, Eagappanath T, Venkatesh N, Jubie S, Samanta MK. Preparation and characterisation of PLGA-nanoparticles containing an anti-hypertensive agent. Int J PharmTech Res, 2009; 1(2):390–3.

Kurose H, Shibata MA, Iinuma M, Otsuki Y. Alterations in cell cycle and induction of apoptotic cell death in breast cancer cells treated with α-mangostin extracted from mangosteen pericarp. J Biomed Biotechnol, 2012; 2012:672428.

Manjunath K, Venkateswarlu V. Pharmacokinetics, tissue distribution and bioavailability of clozapine solid lipid nanoparticles after intravenous and intraduodenal administration. J Control Release, 2005; 107(2):215–28.

Mehnert W, Mader K. Solid lipid nanoparticles: production, characterization and applications. Adv Drug Deliv Rev, 2001; 47(2–3):165–96.

Mills T, Roberson JC. Instrumental data for drug analysis. 1st edition, CRC Press, Boca Raton, FL, 1993.

Mohtar N, Khan NAK, Darwis Y. Solid lipid nanoparticles of atovaquone based on 24 full-factorial design. Iran J Pharm Res, 2015; 14:989–1000.

Muchow M, Maincent P, Muller RH. Lipid nanoparticles with a solid matrix (SLN, NLC, LDC) for oral drug delivery. Drug Dev Ind Pharm, 2008; 34(12):1394–405.

Muller RH, Keck CM. Challenges and solutions for the delivery of biotech drugs-a review of drug nanocrystal technology and lipid nanoparticles. J Biotechnol, 2004; 113(1–3):151–70.

Muller RH, Mader K, Gohla S. Solid lipid nanoparticles (SLN) for controlled drug delivery—a review of the state of the art. Eur J Pharm Biopharm, 2000; 50(1):161–77.

Neves AR, Lucio M, Martins S, Lima JL, Reis S. Novel resveratrol nanodelivery systems based on lipid nanoparticles to enhance its oral bioavailability. Int J Nanomed, 2013; 8:177–87.

Padhye SG, Nagarsenker MS. Simvastatin solid lipid nanoparticles for oral delivery: formulation development and *in vivo* evaluation. Indian J Pharm Sci, 2013; 75(5):591–8.

Pani NR, Nath LK, Acharya S. Compatibility studies of nateglinide with excipients in immediate release tablets. Acta Pharm, 2011; 61(2):237–47.

Pizzol CD, Filippin-Monteiro FB, Restrepo JA, Pittella F, Silva AH, Alves de Souza P, Machado de Campos A, Creczynski-Pasa TB. Influence of surfactant and lipid type on the physicochemical properties and biocompatibility of solid lipid nanoparticles. Int J Environ Res Public Health, 2014; 11(8):8581–96.

Savic Gajic I, Savic I, Boskov I, Zerajic S, Markovic I, Gajic D. Optimization of ultrasound-assisted extraction of phenolic compounds from black locust (*Robiniae pseudoacaciae*) flowers and comparison with conventional methods. Antioxidants (Basel), 2019; 8(8):248.

Schwarz JC, Klang V, Karall S, Mahrhauser D, Resch GP, Valenta C. Optimisation of multiple W/O/W nanoemulsions for dermal delivery of aciclovir. Int J Pharm, 2012; 435(1):69–75.

Seyfoddin A, Al-Kassas R. Development of solid lipid nanoparticles and nanostructured lipid carriers for improving ocular delivery of alpha-mangostin. Drug Dev Ind Pharm, 2012; 39(4):508–19.

Shah RM, Eldridge DS, Palombo E, Harding I. Optimization and stability assessment of solid lipid nanoparticles using particle size and zeta potential. J Phys Sci, 2014; 25(1):59–75.

Silva A, Kumar A, Wild W, Ferreira D, Santos D, Forbes B. Long-term stability, biocompatibility and oral delivery potential of risperidone-loaded solid lipid nanoparticles. Int J Pharm, 2012; 436(1–2):798–805.

Silva AC, Gonzalez-Mira E, Garcia ML, Egea MA, Fonseca J, Silva R, Santos D, Souton EB, Ferreira D. Preparation, characterization and biocompatibility studies on risperidone-loaded solid lipid nanoparticles (SLN): high pressure homogenization versus ultrasound. Colloids Surf B Biointerfaces, 2011; 86(1):158–65.

Souto EB, Anselmi C, Centini M, Muller RH. Preparation and characterization of n-dodecyl-ferulate-loaded solid lipid nanoparticles (SLN). Int J Pharm, 2005; 295(1–2):261–8.

Syamsudin, Faizatun, Rahayu L. HPLC analysis and pharmacokinetic study of mangostin after orally administration in rats. Int J Pharm Bio Sci, 2010; 1:1–7.

Vivek K, Reddy H, Murthy RSR. Investigations of the effect of the lipid matrix on drug entrapment, *in vitro* release, and physical stability of olanzapine-loaded solid lipid nanoparticles. AAPS PharmSciTech, 2007; 8(1):16–24.

Wathoni N, Rusdin A, Motoyama K, Joni IM, Lesmana R, Muchtaridi M. Nanoparticle drug delivery systems for α-mangostin. Nanotechnol Sci Appl, 2020; 13:23–36.

Westesen K, Siekmann B, Koch MH. Investigations on the physical state of lipid nanoparticles by synchrotron radiation X-ray diffraction. Int J Pharm, 1993; 93:189–99.

Zainol S, Basri M, Basri HB, Shamsuddin AF, Abdul-Gani SS, Karjiban RA, Abdul-Malek E. Formulation optimization of a palm-based nanoemulsion system containing levodopa. Int J Mol Sci, 2012; 13(10):13049–64.

Zhao Y, Tang G, Tang Q, Zhang J, Hou Y, Cai E, Liu S, Lei D, Zhang L, Wang S. A method of effectively improved α-mangostin bioavailability. Eur J Drug Metab Pharmacokinet, 2016; 41(5):605–13.

Zirak M, Pezeshki A. Effect of surfactant concentration on the particle size, stability and potential zeta of beta carotene nano lipid carrier. Int J Curr Microbiol App Sci, 2015; 4(9):924–32.

How to cite this article:
Babu VN, Rao GSNK, Budha RR, Alavala RR, Desu PK, Babu GK, Prasad AD. Development, characterization and optimization of solid lipid nanoparticles of alpha-mangostin by central composite design approach. J Appl Pharm Sci, 2023; 13(08):140–150.